Journal of Applied Hydrography

HYDROGRAPHISCHE NACHRICHTEN 03/2026 HN 133

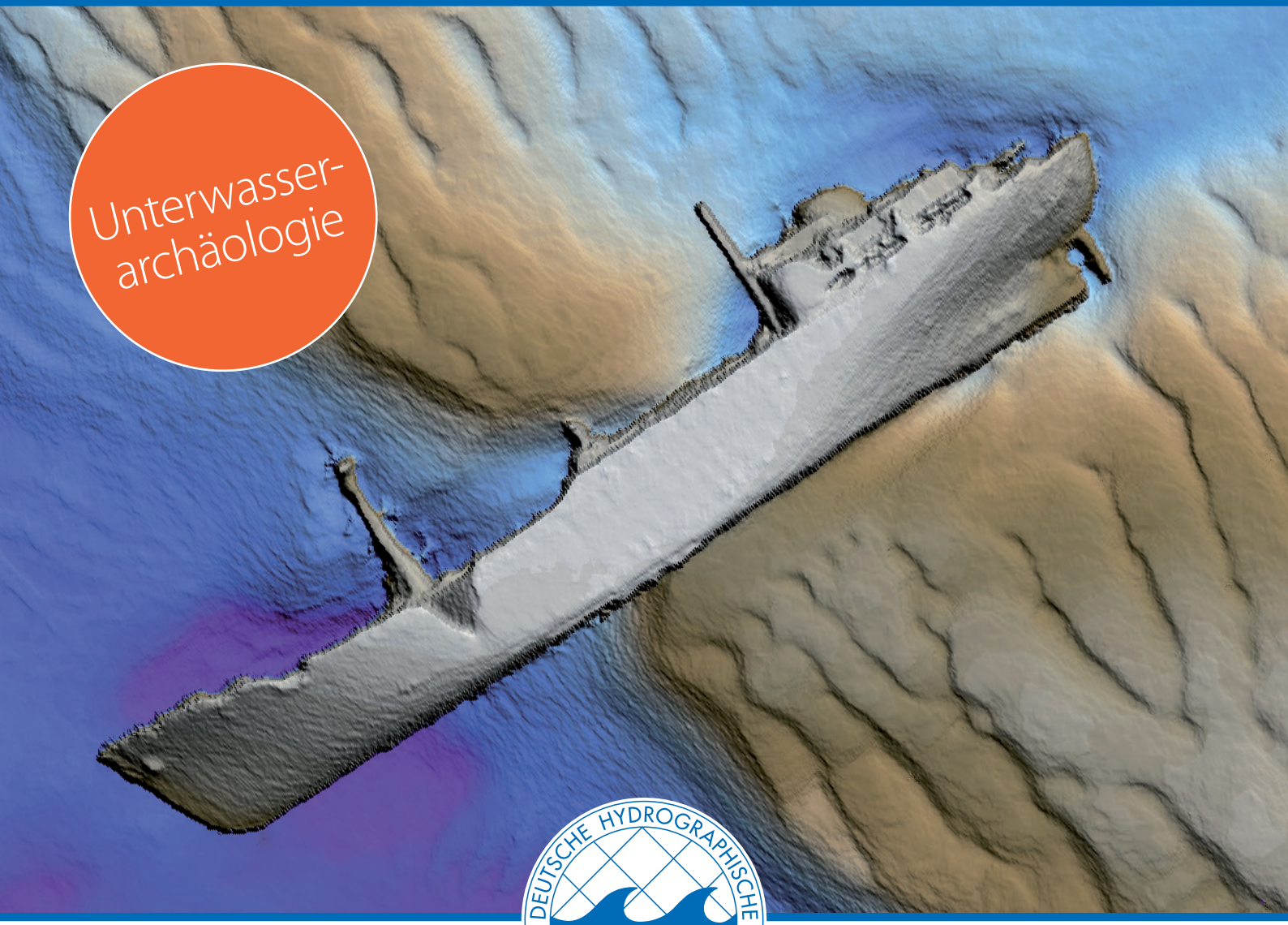

DEUTSCHE HYDROGRAPHISCHE GESELLSCHAFT e.V.
DHyG

DOI: 10.23784/HN133-09

The influence of seamount morphology on sediment accumulation and its potential reflection in the upper-ocean currents

An article by JOSY A. BERGMANN

Seamounts (SM) influence sedimentary depositions as well as oceanic currents, shaping the surrounding biota and increasing biological diversity as well as variability. This study investigates how seamount morphology steers sediment distribution and how these patterns may be reflected in upper water column current measurements. Five seamounts, located in two areas (SMA 16-17 and SMA 18-19-20), were underway surveyed during the MSM 140/2 transit cruise of the research vessel (RV) *Maria S. Merian,* using vessel-mounted multibeam echo sounder (MBES), sub-bottom profiler (SBP) and acoustic doppler current profiler (ADCP). The seafloor was characterised using automated geomorphon classification, while the sedimentary properties were analysed using automated MBES segmentation based on bathymetry data and backscatter intensities along with the evaluation of SBP echograms. In both study sites, the sediment accumulation correlates to the seamount morphology. The ADCP measurements show variability in zonal and meridional velocities within the upper 200 to 300 m, implying consistency with global currents but not sufficient to relate the measurements to the focus areas.

bathymetry | ocean currents | seamounts | sediment transport | underway survey
Bathymetrie | Meeresströmungen | Seamounts | Sedimenttransport | Transitvermessung

Seamounts (SM) beeinflussen Sedimentablagerungen und Meeresströmungen, wodurch sie das umgebende Ökosystem prägen und die biologische Vielfalt sowie Variabilität erhöhen. Diese Studie untersucht, wie die Morphologie von Seamounts die Sedimentverteilung steuert und wie sich diese Muster in Strömungsmessungen der oberen Wassersäule widerspiegeln können. Fünf Seamounts, die in zwei Studiengebieten (SMA 16-17 und SMA 18-19-20) liegen, wurden während der Transitfahrt MSM 140/2 des Forschungsschiffs (FS) *Maria S. Merian* mit einem schiffsmontierten Fächerecholot (MBES), Sub-Bottom Profiler (SBP) und einem Acoustic Doppler Current Profiler (ADCP) untersucht. Der Meeresboden wurde mit Hilfe einer automatisierten geomorphologischen Klassifizierung charakterisiert, während die Sedimenteigenschaften anhand einer automatisierten MBES-Segmentierung (basierend auf Bathymetriedaten und Rückstreuintensitäten) sowie der Auswertung von SBP-Echogrammen analysiert wurden. In beiden Untersuchungsgebieten korreliert die Sedimentakkumulation mit der Morphologie der Seamounts. Die ADCP-Messungen zeigen Schwankungen in den zonalen und meridionalen Geschwindigkeiten innerhalb der oberen 200 bis 300 m, was auf eine Übereinstimmung mit den globalen Strömungen hindeutet, jedoch nicht ausreicht, um die Messungen mit den Studienbereichen in Verbindung zu bringen.

Author
Josy Bergmann studies Hydrography at HafenCity University in Hamburg.

josy.bergmann@hcu-hamburg.de

Introduction

Seamounts represent one of the most predominant structures of the deep-ocean landscape (Mohn et al. 2018). The International Hydrographic Organization (2019) provides a standardised definition of seamounts as follows: »A distinct generally equidimensional elevation greater than 1,000 m above the surrounding relief as measured from the deepest isobath that surrounds most of the feature.« SMs influence local as well as global oceanic currents by redistributing energy from surface tides, blocking water flow and creating eddies (Buchs et al. 2014). Deep-ocean currents typically reach velocities of about 1 to 2 cm/s and are a driving factor for re-mobilising sediments, diffusing organisms and microplastics, and affecting benthic habitats (Turnewitsch et al. 2013; Frey et al. 2025). The interaction between deep-ocean

currents and sediment dynamics shapes the surrounding biota and increases biological diversity as well as variability (Iyer et al. 2012; Mohn et al. 2021).

Studies of Joo et al. (2020) and Gao et al. (2025) explored sediment distribution around seamounts in the Western Pacific, combining data from MBES with deep-towed camera systems. Joo et al. (2020) showed that high backscatter intensities and steep slopes are associated with exposed bedrock, while Gao et al. (2025) found an increase of sediment cover downslope from summit to flank and base. Integrating the influence of bottom currents on the sedimentary distribution, Frey et al. (2025) determined that areas of variable bedforms in the sediments are associated with bottom currents and topographic interactions. Wilckens (2023) also investigated on the interactions between ocean currents and sedimentary system, showing higher speeds and steeper slopes favour secondary flow.

During the transit cruise (MSM 140/2) of the *RV Maria S. Merian* from Brest, France to Rio de Janeiro, Brazil, several seamounts were surveyed underway at speeds of 10 to 12 knots, using vessel-mounted MBES, SBP and ADCP. This study focuses on two areas comprising five seamounts in order to investigate how seamount morphology influences sediment distribution and its potential reflection in upper-ocean currents. The seamount area (SMA) 16-17 consists of two previously charted seamounts (SM 16, SM 17), whereas the SMA 18-19-20 area includes three seamounts, of which two (SM 19, SM 20) had been charted prior to this survey and one (SM 18) had not. Both lie within the formation zone of the Brazil Current (BC), which originates south of 10°S, transporting warm, high-salinity Atlantic Tropical Water southwards within the upper 200 m (Pereira et al. 2014).

Methodology

Data acquisition

The EM124 (MBES by Kongsberg) operates at a fixed frequency of 12 kHz to collect bathymetric information of the seafloor. Given the absence of in-situ sound velocity profiles, data from the World Ocean Atlas 2023 were utilised instead (Garcia et al. 2024).

To gather profiles of the submarine strata a P70 (SBP by Teledyne) was used. The system operated with primary high-frequency (PHF) channels at 18 kHz and 21 kHz. Single acoustic pulses were transmitted at a pulse repetition interval of 100 ms, using a continuous wave pulse type.

The ADCP instrument used (OceanSurveyor by Teledyne) recorded the current velocities in the upper water column at operating frequencies of 38 kHz (depth range of approximately 700 m) and 75 kHz (depth range of about 1000 m). Both systems acquired data in single-ping narrowband mode.

Data processing

The software Qimera from QPS B.V. was utilised to post-process the acquired bathymetry data. The analysis on the morphology of the survey areas was done using the software FMGT by QPS B.V. as well as the software QGIS with the toolbox GRASS GIS and plug-in MarineTools. The tool r.geomorphon (GRASS GIS) was employed for automated classification of the terrain. Geomorphons present terrain forms, such as slopes, ridges, shoulders, valleys and flats, which are derived using a machine-vision approach based on an eight-tuple pattern of visibility neighbourhood. The MBES also recorded backscatter intensities, which were processed in FMGT to produce backscatter mosaics. The generated mosaics were used as an input for the MBES Segmentation (MarineTools). The MBES Segmentation creates a set of vector polygons that represent coherent regions derived from the statistics of the input data. From the bathymetry input, slope and terrain roughness derivatives are determined. Along with the backscatter mosaic, an Object Based Image Analysis is performed based on k-means clustering. Each class is assigned statistical attributes, namely the (normalised) mean and standard deviation of backscatter intensity, slope and terrain roughness (Le Bas n.d.).

The acquired echogram profiles of the SBP were replayed on board the *RV Maria S. Merian* using the acquisition software. For further analysis of stratification thickness, the software SonarWIZ by Chesapeake Technology was employed.

In MatLab, the GEOMAR Toolbox was used to post-process the ADCP data. Processing included data quality control, exclusion of bins with insufficient valid measurements (<25 %), correction for vessel motion and removal of hydroacoustic interference before averaging into 60 seconds ensembles.

Results

The geomorphon classification of SMA 16-17 (Fig. 1) reveals three peak areas. Each peak is surrounded by a concentric pattern of ridges, which transition outward into spurs and slopes. This geomorphic pattern is most developed around SM 16 and SM 17. The area around SM 17 is dominated by footslopes, marking the transition from SM 17 to the elevation opposite. Within this transition zone, a flat surface is primarily present.

In SMA 18-19-20 (Fig. 2) three peaks are identified. A pronounced valley structure prevails the area around SM 18 and is partially corroded by footslopes. This valley structure is bounded by hollow and slope structures, which are particularly evident in the central part of the survey swath. SM 20 is equally characterised by surrounding valley structure, whereas SM 19 shows contrasting morphology. The area between SM 18 and SM 19-20

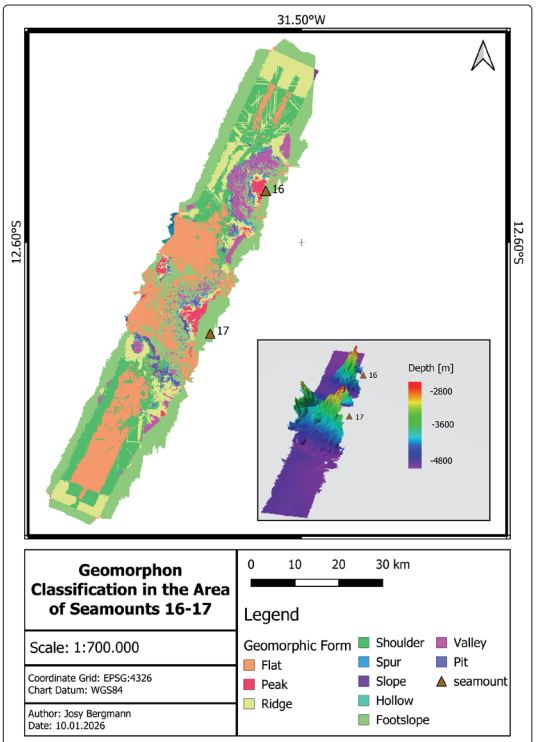

Fig. 1: Overview map of the classified geomorphons of SMA 16-17

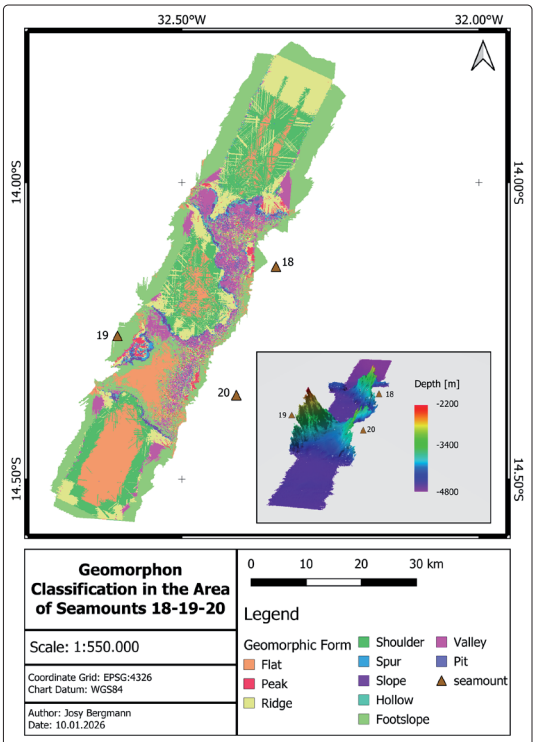

Fig. 2: Overview map of the classified geomorphons in SMA 18-19-20

is marked by ridges, which change into shoulder structures and ultimately into a flat area (Fig. 2).

In SMA 16-17, backscatter intensities range from –66 dB to –20 dB, and the MBES Segmentation resulted in eleven classes (Fig. 3). The lower backscatter values, between –48 dB and –55 dB, occur north and south of the seamount structures. The topographic highs of SM 16 and SM 17 are categorised into class 6.0, representing high mean backscatter values together with a low mean slope and higher mean roughness values. Areas surrounding the seamounts are assigned to class 19.0 with comparatively lower mean backscatter values, a moderate mean slope and high roughness values.

Within the SMA 18-19-20, the MBES Segmentation resulted in twelve classes. SM 18 and SM 20 are predominantly covered by class 5.0, which is characterised by higher mean backscatter, slope and roughness values. This is also observed for SM 19, although over a smaller spatial extent. The transition zone between SM 19 and SM 20 is primarily covered by class 0.0, presenting lower mean backscatter intensities and roughness values.

Approaching SM 16, the sub-bottom stratification shows a regular pattern of reflector layers (Fig. 4). At location (a), the penetration depth is 94.81 m and decreases towards the mount to approximately 45.25 m (location (b)). The steep elevation of SM 16 shows no signal penetration. Immediately south of SM 16, a depression with a penetration depth of 55.25 m (location (c)) is present. It has a regular, continuous reflection and a circularly bounded geometry. Between SM 16 and SM 17, a thin but continuous reflection layer is observed. This layer decreases from 30.29 m to 18.20 m towards SM 17, before no reflections are detected on the flanks of SM 17. The highest surveyed part of SM 17 shows partial reflections. Beyond SM 17, thin sub-bottom reflectors are observed with increasing thickness at a distance of about 40 km from SM 17.

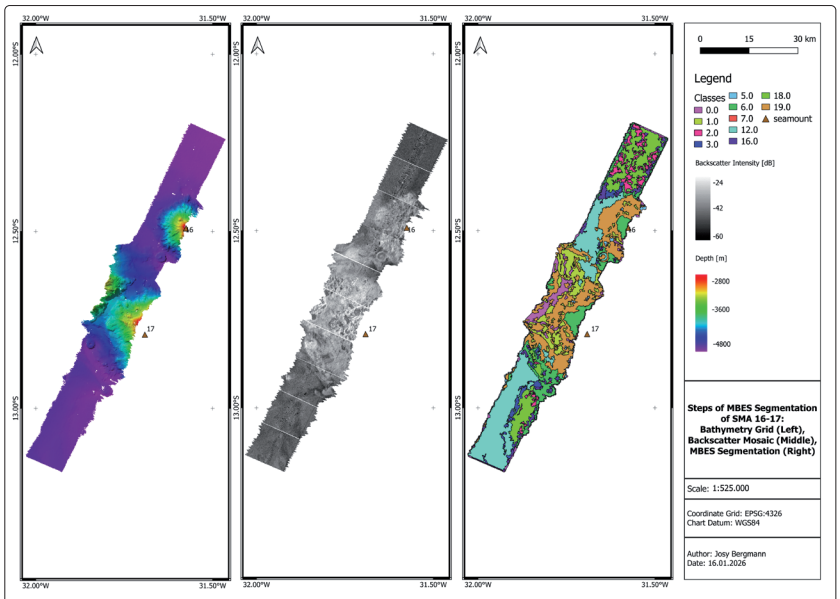

Fig. 3: Overview map of the bathymetry grid (left), the backscatter mosaic (middle) and the MBES Segmentation (right) of SMA 16-17

The echogram for the SM 18-19-20 survey area shows continuous, layered reflectors upon approaching SM 18 (Fig. 5). These reflections thin out and largely disappear when passing over the SM 18, where only weak to no sub-bottom penetration is observed. In the area between SM 18 and SM 19-20, there are layered reflections with a signal penetration depth of 97.84 m (location (a)). North of the transition zone between SM 19 and SM 20, no signal reflection can be seen. When reaching the highest part of the zone and continuing downslope, penetration depth partially increases on flatter parts and is characterised by strong continuous reflectors.

Between 1 November 2025, 20:21.53 UTC and 2 November 2025, 00:51.53 UTC, the study area of SM 16-17 was surveyed. SMA 18-19-20 were investigated on 2 November 2025, from 04:51.53 UTC to 08:21.53 UTC. Fig. 6 shows the zonal and meridional velocities of the 75 kHz ADCP from 31 October 2025, 21:00 UTC to 2 November 2025, 21:00 UTC. In the SM 16-17 area, zonal velocities range from –0.48 m/s to 0.25 m/s. Lower zonal velocities mainly occur in the upper 300 m of the water column, while comparatively higher values are observed below this depth. Meridional velocities in the SMA 16-17 increase over time, with higher values present in the upper 400 m and maximum of 0.36 m/s. In the SMA 18-19-20, greater zonal velocities are examined down to approximately 200 m, with a maximum of 0.37 m/s. The meridional velocities of this area decrease with time.

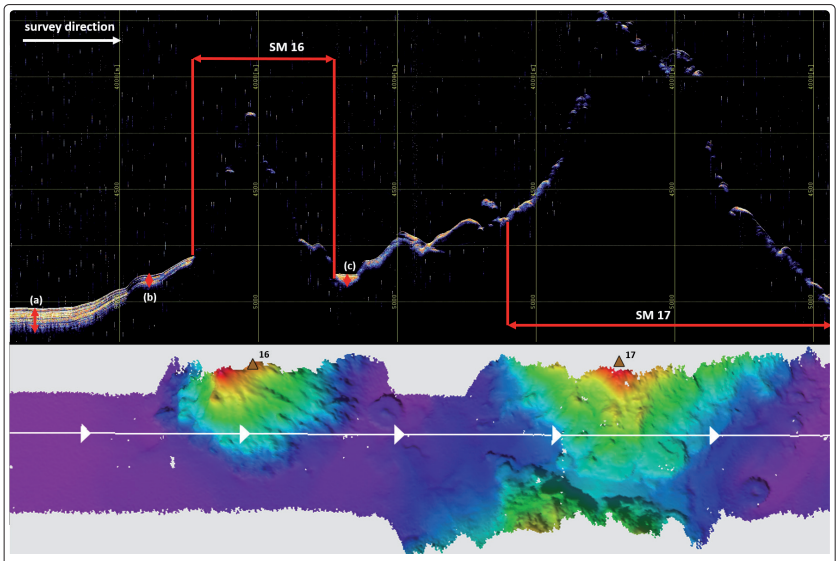

Fig. 4: Echogram profile of the sub-bottom stratification along with the DTM of SMA 16-17 (modified screen capture in Atlas Parastore)

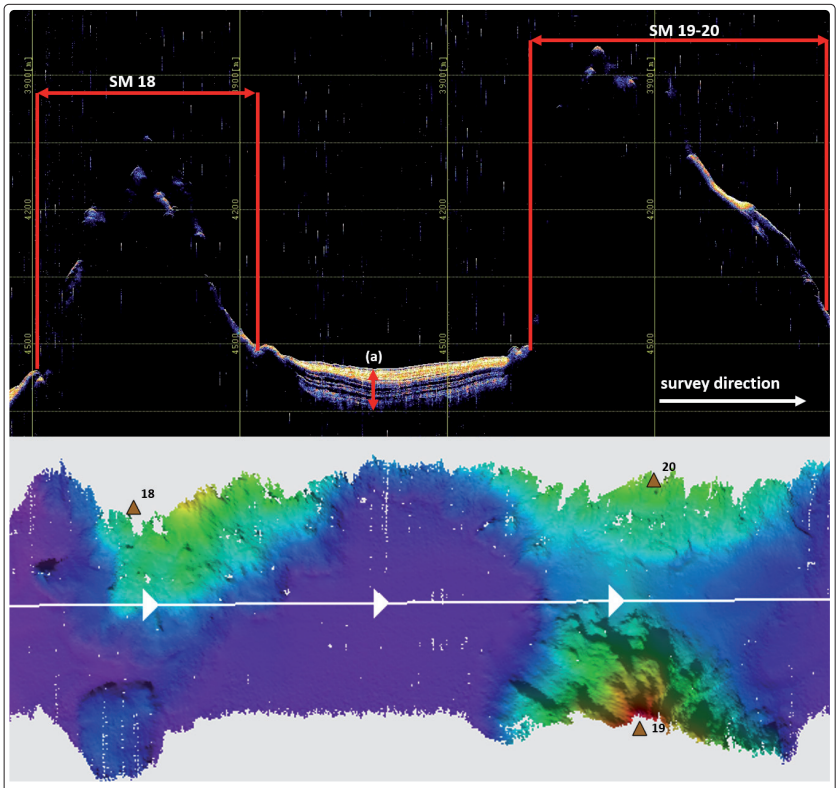

Fig. 5: Echogram profile of the sub-bottom stratification along with the DTM of SMA 18-19-20 (modified screen capture in Atlas Parastore)

Discussion

The observed sediment distribution in the focus areas of SMA 16-17 and SMA 18-19-20 show spatial coherence with seamount morphology, indicating depositional and erosional patterns. In SMA 16-17, sediments predominantly accumulate on shoulders and flats characterised by mean, low terrain roughness and relatively mean, low backscatter intensities, whereas the topographic highs show little to no sub-bottom penetration and are associated with higher backscatter values, indicating hard and exposed substrates (Joo et al. 2020). This contrast between sediment-covered flat regions and the weakly sedimented highs coincides with findings of Joo et al. (2020) and Gao et al. (2025). This suggests accelerating bottom currents over seamounts and steep relief, leading to erosion, while lower speeds are present on flatter surfaces, favouring sediment accumulation (Turnewitsch et al. 2013; Wilckens 2023). Immediately downstream of SM 16, a local entrapment of sediments within a ridge is observed, suggesting lee-side deposition where flow decelerates after passing the flank. SMA 16-17 is, comparatively, topographically open structured (cf. SMA 18-19-20), as the area in-between SM 16 and SM 17 is not bound by slopes, ridges and hollows, but rather dominated by elongated flats, bisected by footslopes towards SM 17. Additionally, water can flow in zonal directions through both seamounts, creating a well-connected topography, which may act as transport pathway rather than a sedimentary depot, explaining the observed thin sediment layer beyond the local entrapment. As SM 17 forms a complex with the opposing elevation, it acts as a morphological barrier that limits sediment accumulation south

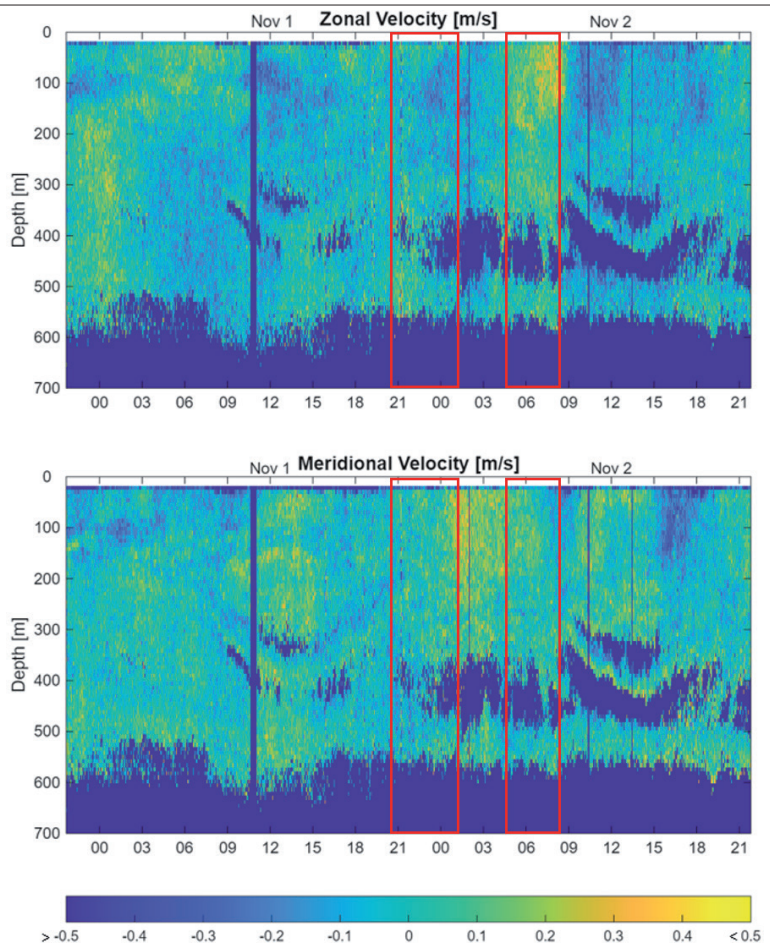

Fig. 6: Plots of zonal and meridional velocities of the 75 kHz ADCP system spanning from 31 October 2025, 21:00 UTC to 2 November 2025, 21:00 UTC (own representation in MatLab)

of the seamount. Increased sediment thickness is first observed about 40 km downstream along the track, where the flow field weakens again as the seafloor becomes more uniform. In contrast, the SMA 18-19-20 exhibits a morphological enclosed structure, in which the mounts are bounded by pronounced spurs, slopes and hollows. Between SM 18 and SM 19-20, the area is dominated by shoulders as well as flats, and the echogram exhibits thick, regularly layered sediment accumulation, indicating sediment entrapment within the basin. This enclosed topography might alter the bottom current pathway through local recirculation, which traps suspended particles within the basin (White and Mohn 2004; Turnewitsch et al. 2013). Once such circulation is established, the current repeatedly reworks the sediment but does not transport it further (Wilckens 2023). In addition, information on the sediment types is important to determine whether observed currents are capable of transporting the material. This was investigated by performing an Angular Response Analysis of MBES backscatter intensities but the method did not deliver reliable results. The measured current velocities cannot be used to directly characterise and validate due to the limited depth range of the ADCP. Nevertheless, the zonal and meridional velocities show variability in the upper 200 m of the water column, specifically in the zonal velocities of SMA 18-19-20 and in the meridional velocities between SMA 16-17 and SMA 18-19-20. Because the study areas are located within the transformation zone of the BC, which transports water southward in the upper 200 m of the water column (Pereira et al. 2014), this variability likely reflects the influence of the BC. To specifically account for the flow directions and quantity of SMA 16-17 and SMA 18-19-20, near bottom current measurements are required. As bottom currents are fluctuating, the observations need to be performed over longer periods of time, e.g. using moored ADCP systems. An alternative approach is the usage of the ARGO float network (cf. Frey et al. 2025).

Conclusion

The results suggest that sediment accumulation is influenced by the morphology of the seamounts. In both sites, the slopes of the mounts showed little to no sediment accumulation, indicating erosion due to accelerated bottom currents. Sediment depositions are dominant on flats of the luv-side before the seamounts, and local entrapments on the lee-side after currents decelerate downslope. SMA 16-17 is characterised by a rather openly structured topography where the area between SM 16 and SM 17 likely acts as sediment pathway. An enclosed topography is exhibited for SMA 18-19-20, suggesting sediment entrapment because of local recirculating bottom currents. The assumptions made on the interaction between bottom currents and sediment depositions could not be validated through ADCP measurements, as no coherent velocities were observed and the measurements likely reflect the southward-flowing BC rather than local seamount driven currents. This study can be viewed as limited as the collected data during MSM 140/2 were acquired during an underway survey, which limited the coverage in terms of survey directions, temporal resolution, survey speed and the possibility to map the seamounts with their surroundings to full spatial extent. //

References

Buchs, David M.; Kaj Hoernle; Ingo Grevemeyer (2014): Seamounts (chapter 34). Encyclopedia of Marine Geosciences. Springer Netherlands, DOI: 10.1007/978-94-007-6644-0_34-1

Frey, Shannon E.; Martin Jutzeler; Rebecca J. Carey; Peter T. Harris (2025): In-situ sedimentary evidence of complex bottom currents at a modern deepwater seamount. Communications Earth & Environment, DOI: 10.1038/s43247-025-02690-7

Gao, Wei; Heshun Wang; Yongfu Sun; Weikun Xu; Yuanyuan Gui (2025): Sediment Distribution and Seafloor Substratum Mapping on the DD Guyot, Western Pacific. Journal of Marine Science and Engineering, DOI: 10.3390/jmse13101904

Garcia, Hernan E.; Zhankun Wang; Courtney Bouchard et al. (2024): World Ocean Atlas 2023: Volume 3: Dissolved Oxygen, Apparent Oxygen Utilization, and Dissolved Oxygen Saturation and 30-year Climate Normal. DOI: 10.25923/rb67-ns53

IHO (2019): Standardization of Undersea Feature Names: Guidelines, Proposal Form, Terminology. Publication B-6, International Hydrographic Organization

Iyer, S. D.; C. M. Mehta; P. Das; N. G. Kalangutkar (2012): Seamounts – characteristics, formation, mineral deposits and biodiversity. Geologica Acta, DOI: 10.1344/105.000001758

Jasiewicz, Jarek; Tomek Stepinski (2025): r.geomorphons. https://grass.osgeo.org/grass84/manuals/r.geomorphon.html

Joo, Jongmin; Seung-Sep Kim; Jee Woong Choi et al. (2020): Seabed Mapping Using Shipboard Multibeam Acoustic Data for Assessing the Spatial Distribution of Ferromanganese Crusts on Seamounts in the Western Pacific. Minerals, DOI: 10.3390/min10020155

Le Bas, T. (n.d.): MBES Segmentation: Manual. Southampton, UK

Mohn, Christian; Anneke Denda; Svenja Christiansen et al. (2018): Ocean currents and acoustic backscatter data from shipboard ADCP measurements at three North Atlantic seamounts between 2004 and 2015. Data Brief, DOI: 10.1016/j.dib.2018.01.014

Mohn, Christian; Martin White; Anneke Denda et all (2021): Dynamics of currents and biological scattering layers around Senghor Seamount, a shallow seamount inside a tropical Northeast Atlantic eddy corridor. Deep Sea Research Part I: Oceanographic Research Papers, DOI: 10.1016/j.dsr.2021.103497

Pereira, Janini; Mariela Gabioux; Martinho Marta-Almeida at all (2014): The Bifurcation of the Western Boundary Current System of the South Atlantic Ocean. Brazilian Journal of Geophysics, DOI: 10.22564/rbgf.v32i2.456

Turnewitsch, Robert; Saeed Falahat; Jonas Nycander et al. (2013): Deep-sea fluid and sediment dynamics – Influence of hill- to seamount-scale seafloor topography. Earth-Science Reviews, DOI: 10.1016/j.earscirev.2013.10.005

White, Martin; Christian Mohn (2004): Seamounts: A review of physical processes and their Influence on the seamount ecosystem. Oceanic Seamounts: An Integrated Study, https://epic.awi.de/id/eprint/37314/17/OASIS_Oceanography.pdf

Wilckens, Henriette (2023): Contourite development: Analysing the interaction between bottom currents and sedimentary systems. Dissertation, University of Bremen